DOI:10.1021/ic802026n

Inorganic Chemistry
Article

Three-Dimensional Metal Azide Coordination Polymers with Amino Carboxylate Coligands: Synthesis, Structure, and Magnetic Properties

Zi-Lu Chen,[†] Chun-Fang Jiang,[†] Wei-Hong Yan,[†] Fu-Pei Liang,*[,†] and Stuart R. Batten[‡]

[†]*School of Chemistry and Chemical Engineering, Guangxi Normal University, Guilin 541004, China and* [‡]*School of Chemistry, Monash University, Victoria 3800, Australia*

Received October 22, 2008

The reaction of M(II) ions with azido ligands in the presence of different amino carboxylic acids gave four three-dimensional metal−azido coordination polymers, $[Mn(3,5\text{-daba})(N_3)]_n$ (**1**), $[Cd(3,5\text{-daba})(N_3)]_n$ (**2**; 3,5-daba = 3,5-diaminobenzoate), $[Mn(4\text{-aba})(N_3)]_n$ (**3**; 4-aba = 4-aminobenzoate), and $[Cu_2(gly)_2(N_3)_2]_n$ (**4**; gly = glycinate), which display different topological structures. Polymers **1** and **2** present 4,6-connected 3D networks with different Schläfli symbols. However, **3** and **4** feature an unprecedented trinodal 3,6-connected network with the Schläfli symbol $(4^2.6)(4.6^2)(4^3.6^6.8^6)$ and an unusual 4-connected 3D net with the Lonsdaleite (hexagonal diamond) topology, respectively. Magnetic susceptibility measurements revealed dominant antiferromagnetic couplings for **1** and **3** and an overall dominant ferromagnetic coupling for **4**, which presents metamagnetic behavior with a magnetic phase transition at a critical temperature of 6 K and a transition field of ca. 6030 Oe. The results demonstrate that the EE azido and syn−anti carboxylato bridges in our cases induce an antiferomagnetic interaction, and the anti−anti carboxylato bridge in **4** mediates a ferromagnetic interaction. The magnetic interaction through the EO azido bridge in **3** and **4** has a dependence on the value of the M−N−M bond angle.

Introduction

The syntheses and properties of metal−azido complexes have attracted great research interest for many years due to their fascinating structural diversities, their importance in understanding magneto-structural correlations, and their promising potential applications in functional materials.[1] A variety of metal−azido complexes with discrete or one-, two-, and three-dimensional structures have been reported, in which the azido ligand exhibits various coordination modes ranging from μ-1,1 (end-on, EO) and μ-1,3 (end-to-end, EE) to μ-1,1,1, μ-1,1,3, μ-1,1,1,1, μ-1,1,3,3, and μ-1,1,1,3,3,3, depending on the steric and electronic demands of the coligands.[2] The magnetic coupling interactions mediated via the azido bridge are found to be affected by the linking modes of the azido ligand. In general, the exchange is ferromagnetic for the EO mode and antiferromagnetic for the EE mode.[3−5] Other interesting magnetic phenomena

*To whom correspondence should be addressed. E-mail: fliangoffice@yahoo.com. Tel.: +86(0)773/5845973. Fax: +86(0)773/5832294.

(1) (a) Bonnet, M. L.; Aronica, C.; Chastanet, G.; Pilet, G.; Luneau, D.; Mathoniere, C.; Clerac, R.; Robert, V. *Inorg. Chem.* **2008**, *47*, 1127–1133. (b) Escuer, A.; Mautner, F. A.; Goher, M. A. S.; Abu-Youssef, M. A. M.; Vicente, R. *Chem. Commun.* **2005**, 605–607. (c) Escuer, A.; Vicente, R.; Goher, M. A. S.; Mautner, F. A. *Inorg. Chem.* **1996**, *35*, 6386–6391. (d) Gao, E. Q.; Yue, Y. F.; Bai, S. Q.; He, Z.; Yan, C. H. *J. Am. Chem. Soc.* **2004**, *126*, 1419–1429. (e) Hong, C. S.; Do, Y. *Angew. Chem., Int. Ed.* **1999**, *38*, 193–195. (f) Liu, C.-M.; Gao, S.; Zhang, D.-Q.; Huang, Y.-H.; Xiong, R.-G.; Liu, Z.-L.; Jiang, F.-C.; Zhu, D.-B. *Angew. Chem., Int. Ed.* **2004**, *43*, 990–994. (g) Murugesu, M.; Habrych, M.; Wernsdorfer, W.; Abboud, K. A.; Christou, G. *J. Am. Chem. Soc.* **2004**, *126*, 4766–4767. (h) Stamatatos, T. C.; Abboud, K. A.; Wernsdorfer, W.; Christou, G. *Angew. Chem., Int. Ed.* **2007**, *46*, 884–888. (i) Wang, X. Y.; Wang, L.; Wang, Z. M.; Su, G.; Gao, S. *Chem. Mater.* **2005**, *17*, 6369–6380. (j) Yang, C. I.; Wernsdorfer, W.; Lee, G. H.; Tsai, H. L. *J. Am. Chem. Soc.* **2007**, *129*, 456–457.

(2) (a) Boudalis, A. K.; Donnadieu, B.; Nastopoulos, V.; Clemente-Juan, J. M.; Mari, A.; Sanakis, Y.; Tuchagues, J.-P.; Perlepes, S. P. *Angew. Chem., Int. Ed.* **2004**, *43*, 2266–2270. (b) Halcrow, M. A.; Huffman, J. C.; Christou, G. *Angew. Chem., Int. Ed.* **1995**, *34*, 889–891. (c) Meyer, F.; Demeshko, S.; Leibeling, G.; Kersting, B.; Kaifer, E.; Pritzkow, H. *Chem.—Eur. J.* **2005**, *11*, 1518–1526. (d) Mialane, P.; Dolbecq, A.; Marrot, J.; Rivière, E.; Sécheresse, F. *Chem.—Eur. J.* **2005**, *11*, 1771–1778. (e) Munno, G. D.; Poerio, T.; Viau, G.; Julve, M.; Lloret, F. *Angew. Chem., Int. Ed.* **1997**, *36*, 1459–1461. (f) Papaefstathiou, G. S.; Perlepes, S. P.; Escuer, A.; Vicente, R.; Font-Bardia, M.; Solans, X. *Angew. Chem., Int. Ed.* **2001**, *40*, 884–886. (g) Ribas, J.; Monfort, M.; Ghosh, B. K.; Cortes, R.; Solans, X.; Font-Bardia, M. *Inorg. Chem.* **1996**, *35*, 864–868. (h) Tuczek, F.; Bensch, W. *Inorg. Chem.* **1995**, *34*, 1482–1486. (i) Wemple, M. W.; Adams, D. M.; Hagen, K. S.; Folting, K.; Hendrickson, D. N.; Christou, G. *J. Chem. Soc., Chem. Commun.* **1995**, 1591–1593. (j) Abu-Youssef, M. A. M.; Langer, V.; Luneau, D.; Shams, E.; Goher, M. A. S.; Öhrström, L. *Eur. J. Inorg. Chem.* **2008**, 112–118. (k) Gao, E.-Q.; Wang, Z.-M.; Yan, C.-H. *Chem. Commun.* **2003**, 1748–1749.

(3) (a) Ribas, J.; Escuer, A.; Monfort, M.; Vicente, R.; Cortés, R.; Lezama, L.; Rojo, T. *Coord. Chem. Rev.* **1999**, *193*−*195*, 1027–1068. (b) Ribas, J.; Monfort, M.; Vicente, R.; Cortes, R.; Lezama, L.; Rojo, T.; Goher, M. A. S. *Magnetism: Molecules to Materials II: Molecule-Based Materials*; Wiley-VCH Verlag GmbH & Co. KGaA: Weinheim, Germany, 2002.

(4) Ruiz, E.; Cano, J.; Alvarez, S.; Alemany, P. *J. Am. Chem. Soc.* **1998**, *120*, 11122–11129.

(5) Tandon, S. S.; Thompson, L. K.; Manuel, M. E.; Bridson, J. N. *Inorg. Chem.* **1994**, *33*, 5555–5570.

Published on Web 4/21/2009

have also been observed in systems with mixed azide bridging modes.[6]

In the field of metal−azido chemistry, the construction of high-dimensional networks of azido-bridged complexes is of particular interest because of their novel topology and potential enhancement of bulk magnetic properties.[7] The common strategies for this purpose reported in the literature include the further extension of metal−azido assemblies by introducing a second bridging ligand[8] or the use of more azido ligands by adding a countercation, such as Cs^+ or $N(CH_3)_4^+$,[9] or by employing chelating diamine ligands, such as ethylenediamine and its derivatives,[10] to alter the network topology. When secondary bridging ligands are used in constructing high-dimensional metal−azido systems, neutral organic ligands have been the most popular, while the use of bridging anionic ligands is relatively rare. Incorporation of bridging anionic ligands into metal−azido systems is still a challenge due to the competition of the negative charged ligand with azide in the self-assembly process.[11,12] Recently, several high-dimensional complexes containing mixed azide and carboxylate bridges have been successfully synthesized.[13,14] The utilization of carboxylate ligands as simultaneous bridges in metal−azido systems is attractive since the carboxylates are well-established ligands in the field of molecular magnetism because of their versatile bridging modes,[15] and such systems featuring mixed azido and carboxylate bridges are good materials for studying the mechanism of magnetic exchange interaction mediated by different superexchange pathways.[16] Amino carboxylic acid ligands feature multiple coordination sites that combine the characteristics of amine and carboxylic groups and are able to exhibit different coordination modes depending on the nature of the reaction system. Therefore, new supramolecular frameworks might be expected for metal−azido complexes with amino carboxylic acid coligands. However, as far as we know, only two diamagnetic Zn(II) and Cd(II) azido complexes with 4-aminobenzoic acid as a bridging coligand have been reported,[17] while high-dimensional paramagnetic coordination polymers with both amino carboxylate and azido bridges have not been reported. Some attempts were made via the reaction of manganese with amino carboxylic acid in the presence of NaN_3; however, these just led to the formation of amino carboxylate complexes without azido ligands present in the final product.[18] Herein, we wish to report the syntheses and structures of four three-dimensional metal−azido coordination polymers with different amino carboxylic acids as second bridging ligands, $[Mn(3,5\text{-daba})(N_3)]_n$ (**1**), $[Cd(3,5\text{-daba})(N_3)]_n$ (**2**; 3,5-daba = 3,5-diaminobenzoate), $[Mn(4\text{-aba})(N_3)]_n$ (**3**; 4-aba = 4-aminobenzoate), and $[Cu_2(gly)_2(N_3)_2]_n$ (**4**; gly = glycinate), and the magnetic properties of **1**, **3**, and **4**. Polymer **4** is the first example of a coordination polymer with a flexible amino acid as a second bridging ligand in metal−azido complexes, and **3** displays an interesting 3,6-connected topology that has not been reported previously.

Experimental Section

Materials and General Methods. All chemicals were used as obtained without further purification. Infrared spectra were recorded as KBr pellets using a Nicolet 360 FT-IR spectrometer. Elemental analyses (C, H, and N) were performed on a Vario EL analyzer. All magnetic measurements including zero-field-cooled and field-cooled magnetizations (ZFCM and FCM, respectively), ac susceptibility measurements, and field-dependent magnetization were carried out on a Quantum Design MPMS-XL SQUID magnetometer. Data were corrected for the diamagnetic contribution calculated from Pascal constants,

(6) (a) Abu-Youssef, M. A. M.; Drillon, M.; Escuer, A.; Goher, M. A. S.; Mautner, F. A.; Vicente, R. *Inorg. Chem.* **2000**, *39*, 5022–5027. (b) Abu-Youssef, M. A. M.; Escuer, A.; Goher, M. A. S.; Mautner, F. A.; Rei, G. J.; Vicente, R. *Angew. Chem., Int. Ed.* **2000**, *39*, 1624–1626. (c) Gao, E. Q.; Bai, S. Q.; Wang, Z. M.; Yan, C. H. *J. Am. Chem. Soc.* **2003**, *125*, 4984–4985. (d) Liu, F. C.; Zeng, Y. F.; Zhao, J. P.; Hu, B. W.; Bu, X. H.; Ribas, J.; Cano, J. *Inorg. Chem.* **2007**, *46*, 1520–1522. (e) Nanda, P. K.; Aromí, G.; Ray, D. *Chem. Commun.* **2006**, 3181–3183.

(7) (a) Escuer, A.; Vicente, R.; Mautner, F. A.; Goher, M. A. S. Abu-Youssef, M. A. M. *Chem.Commun.* **2002**, 64–65. (b) Fu, A.; Huang, X.; Li, J.; Yuen, T.; Lin, C. L. *Chem.—Eur. J.* **2002**, *8*, 2239–2247. (c) Li J.-R.; Yu, Q.; Sañudo, E. C.; Tao, Y.; Bu, X.-H. *Chem. Commun.* **2007**, 2602–2604. (d) Liu, T. F.; Fu, D.; Gao, S.; Zhang, Y. Z.; Sun, H. L.; Su, G.; Liu, Y. J. *J. Am. Chem. Soc.* **2003**, *125*, 13976–13977. (e) Ma, B. Q.; Sun, H. L.; Gao, S.; Su, G. *Chem. Mater.* **2001**, *13*, 1946–1948. (f) Zhang, Y.-Z.; Wernsdorfer, W.; Pan, F.; Wang, Z.-M.; Gao, S. *Chem. Commun.* **2006**, 3302–3304.

(8) (a) Escuer, A.; Cano, J.; Goher, M. A. S.; Journaux, Y.; Lloret, F.; Mautner, F. A.; Vicente, R. *Inorg. Chem.* **2000**, *39*, 4688–4695. (b) Konar, S.; Zangrando, E.; Drew, M. G. B.; Mallah, T.; Ribas, J.; Chaudhuri, N. R. *Inorg. Chem.* **2003**, *42*, 5966–5973. (c) Wang, X. Y.; Wang, L.; Wang, Z. M.; Gao, S. *J. Am. Chem. Soc.* **2006**, *128*, 674–675.

(9) (a) Goher, M. A. S.; Cano, J.; Journaux, Y.; Abu-Youssef, M. A. M.; Mautner, F. A.; Escuer, A.; Vicente, R. *Chem.—Eur. J.* **2000**, *6*, 778–784. (b) Mautner, D. F. A.; Cortés, D. R.; Lezama, D. L.; Rojo, P. T. *Angew. Chem., Int. Ed.* **1996**, *35*, 78–80. (c) Mautner, F. A.; Hanna, S.; Cortes, R.; Lezama, L.; Barandika, M. G.; Rojo, T. *Inorg. Chem.* **1999**, *38*, 4647–4652.

(10) (a) Gu, Z.-G.; Zuo, J.-L.; You, X.-Z. *Dalton Trans.* **2007**, 4067–4072. (b) Mondal, K. C.; Mukherjee, P. S. *Inorg. Chem.* **2008**, *47*, 4215–4225.

(11) (a) Goher, M. A. S.; Youssef, A. A.; Mautner, F. A. *Polyhedron* **2006**, *25*, 1531–1536. (b) Han, Y.-F.; Wang, T.-W.; Song, Y.; Shen, Z.; You, X.-Z. *Inorg. Chem. Commun.* **2008**, *11*, 207–210. (c) Li, L.; Liao, D.; Jiang, Z.; Yan, S. *Polyhedron* **2001**, *20*, 681–684. (d) Li, L.; Liao, D.; Jiang, Z.; Yan, S. *J. Mol. Struct.* **2001**, *597*, 157–162. (e) Tangoulis, V.; Panagoulis, D. Raptopoulou, C. P.; Dendrinou-Samara, C. *Dalton Trans.* **2008**, 1752–1760.

(12) Thompson, L. K.; Tandon, S. S.; Lloret, F.; Cano, J.; Julve, M. *Inorg. Chem.* **1997**, *36*, 3301–3306.

(13) (a) Cheng, L.; Zhang, W.-X.; Ye, B.-H.; Lin, J.-B.; Chen, X.-M. *Eur. J. Inorg. Chem.* **2007**, 2668–2676. (b) Liu, F. C.; Zeng, Y. F.; Jiao, J.; Li, J. R.; Bu, X. H.; Ribas, J.; Batten, S. R. *Inorg. Chem.* **2006**, *45*, 6129–6131. (c) Liu, F. C.; Zeng, Y. F.; Zhao, J. P.; Hu, B. W.; Sanudo, E. C.; Ribas, J.; Bu, X. H. *Inorg. Chem.* **2007**, *46*, 7698–7700. (d) Liu, F.-C.; Zeng, Y.-F.; Zhao, J.-P.; Hu, B.-W.; Bu, X.-H.; Ribas, J.; Batten, S. R. *Inorg. Chem. Commun.* **2007**, *10*, 129–132. (e) Sengupta, O.; Chakrabarty, R.; Mukherjee, P. S. *Dalton Trans.* **2007**, 4514–4516. (f) Zeng, Y. F.; Li, J. R.; Bu, X. H.; Ribas, J.; Bu, X. *Inorg. Chem.* **2005**, *44*, 7298–7300. (g) Zeng, Y.-F.; Liu F.-C.; Zhao, J.-P.; Cai, S.; Bu, X.-H.; Ribas, J. *Chem. Commun.* **2006**, 2227–2229. (h) Liu, F. C.; Zeng, Y. F.; Jiao, J.; Bu, X. H.; Ribas, J.; Batten, S. R. *Inorg. Chem.* **2006**, *45*, 2776–2778.

(14) He, Z.; Wang, Z. M.; Gao, S.; Yan, C. H. *Inorg. Chem.* **2006**, *45*, 6694–6705.

(15) (a) Bai, Y. L.; Tao, J.; Wernsdorfer, W.; Sato, O.; Huang, R. B.; Zheng, L. S. *J. Am. Chem. Soc.* **2006**, *128*, 16428–16429. (b) McInnes, E. J. L.; Pidcock, E.; Oganesyan, V. S.; Cheesman, M. R.; Powell, A. K.; Thomson, A. J. *J. Am. Chem. Soc.* **2002**, *124*, 9219–9228. (c) Mishra, A.; Wernsdorfer, W.; Abboud, K. A.; Christou, G. *J. Am. Chem. Soc.* **2004**, *126*, 15648–15649. (d) Psomas, G.; Raptopoulou, C. P.; Iordanidis, L.; Dendrinou-Samara, C.; Tangoulis, V.; Kessissoglou, D. P. *Inorg. Chem.* **2000**, *39*, 3042–3048. (e) Sessoli, R.; Tsai, H. L.; Schake, A. R.; Wang, S.; Vincent, J. B.; Folting, K.; Gatteschi, D.; Christou, G.; Hendrickson, D. N. *J. Am. Chem. Soc.* **1993**, *115*, 1804–1816. (f) Soler, M.; Wernsdorfer, W.; Folting, K.; Pink, M.; Christou, G. *J. Am. Chem. Soc.* **2004**, *126*, 2156–2165. (g) Tasiopoulos, A. J.; Wernsdorfer, W.; Moulton, B.; Zaworotko, M. J.; Christou, G. *J. Am. Chem. Soc.* **2003**, *125*, 15274–15275. (h) Zheng, Y.-Z.; Tong, M.-L.; Zhang, W.-X.; Chen, X.-M. *Angew. Chem., Int. Ed.* **2006**, *45*, 6310–6314.

(16) (a) Escuer, A.; Vicente, R.; Mautner, F. A.; Goher, M. A. S. *Inorg. Chem.* **1997**, *36*, 1233–1236. (b) Zeng, Y.-F.; Zhao, J.-P.; Hu, B.-W.; Hu, X.; Liu, F.-C.; Ribas, J.; Ribas-Ariño, J.; Bu, X.-H. *Chem.—Eur. J.* **2007**, *13*, 9924–9930.

(17) Chen, H.-J.; Chen, X.-M. *Inorg. Chim. Acta* **2002**, *329*, 13–21.

(18) (a) Wang, R.; Gao, E.; Hong, M.; Gao, S.; Luo, J.; Lin, Z.; Han, L.; Cao, R. *Inorg. Chem.* **2003**, *42*, 5486–5488. (b) Wang, R.; Yuan, D.; Jiang, F.; Han, L.; Gao, S.; Hong, M. *Eur. J. Inorg. Chem.* **2006**, 1649–1656.

and the diamagnetism of the sample and sample holder were taken into account.

Caution! *Azide complexes are potentially explosive. The experiments were carried out in an isolated room, and experimenters should be equipped with safeguards. Only a small amount of the materials should be prepared and handled with great care.*

Synthesis of [Mn(3,5-daba)(N_3)]$_n$ (1). A mixture of 3, 5-diaminobenzoic acid (0.0760 g, 0.5 mmol), $MnCl_2 \cdot 4H_2O$ (0.0980 g, 0.5 mmol), NaN_3 (0.0650 g, 1 mmol), EtOH (3 mL), and H_2O (1 mL) was sealed in a 25 mL Teflon-lined autoclave and heated at 393 K for 6 days. Then, the autoclave was slowly cooled to room temperature, giving brown block crystals of **1**. Yield: 38%. Anal. calcd for $C_7H_7MnN_5O_2$: C, 33.89; H, 2.84; N, 28.23. Found: C, 33.56; H, 2.58; N, 28.04%. IR (KBr, cm^{-1}): 3442(w), 3347(m), 3285(m), 3159(w), 2110(vs), 2088(vs), 1576 (s), 1413(s), 1331(w), 1172(w), 1014(m), 975(m), 932(m), 881(m), 783(m), 760(m), 689(w), 537(w).

Synthesis of [Cd(3,5-daba)(N_3)]$_n$ (2). A mixture of 3,5-diaminobenzoic acid (0.0760 g, 0.5 mmol), $CdCl_2 \cdot 2.5H_2O$ (0.1140 g, 0.5 mmol), NaN_3 (0.0650 g, 1 mmol), and H_2O (2 mL) was sealed in a 25 mL Teflon-lined autoclave and heated at 373 K for 3 days. Then, the autoclave was cooled to room temperature over a period of 24 h. Brown block crystals of **2** were obtained. Yield: 52%. Anal. calcd for $C_7H_7CdN_5O_2$: C, 27.51; H, 2.31; N, 22.92. Found: C, 27.27; H, 2.47; N, 22.63%. IR (KBr, cm^{-1}): 3337(m), 3313(m), 3262(m), 2042(vs), 1544(s), 1399(s), 1329(w), 1062(m), 969(m), 942(w), 795(m), 772(m), 681(w), 494(w).

Synthesis of [Mn(4-aba)(N_3)]$_n$ (3). A mixture of 4-aminobenzoic acid (0.0685 g, 0.5 mmol), $MnCl_2 \cdot 4H_2O$ (0.098 g, 0.5 mmol), NaN_3 (0.0975 g, 1.5 mmol), ethanol (4 mL), and water (0.5 mL) was placed in a 25-mL Teflon-lined autoclave and heated at 393 K for 7 days. Then, it was cooled down slowly to room temperature, giving brown needle crystals of **3** in a yield of 40%. Anal. calcd for $C_7H_6MnN_4O_2$: C, 36.07; H, 2.59; N, 24.04. Found: C, 36.20; H, 2.47; N, 24.27%. IR (KBr, cm^{-1}): 3412(w), 3336(m), 3265(m), 2078(s), 1608(s), 1551(s), 1516(s), 1398(s), 1241(w), 1179(w), 1099(w), 987(m), 966(m), 860(w), 852(w), 790(m), 703(w), 653(w), 621(m), 548(m).

Synthesis of [Cu_2(gly)$_2$(N_3)$_2$]$_n$ (4). A solution of NaN_3 (0.0195 g, 0.3 mmol) in 2 mL of ethanol and 1 mL of water was added slowly into a solution of $Cu(NO_3)_2 \cdot 3H_2O$ (0.1449 g, 0.6 mmol) and gly (0.0450 g, 0.6 mmol) in 10 mL of water. The pH value of the solution was adjusted to 6.4 by adding 0.1 $mol \cdot L^{-1}$ NaOH. The resulted solution was stirred at room temperature for 2 h and then placed in a refrigerator to give green crystals after two weeks in a yield of 58%. Anal. calcd for $C_4H_8Cu_2N_8O_4$: C, 13.37; H, 2.24; N, 31.19. Found: C, 13.65; H, 2.15; N, 31.30%. IR (KBr, cm^{-1}): 3352(m), 3284(m), 2111(s), 2056(m), 1617(s), 1428(w), 1379(m), 1299(w), 1106(w), 1041(w), 915(w), 739(w), 594(w).

X-Ray Crystallography. The selected single crystals of **1**−**4** were put in a sealed tube, and the measurement was performed on a Bruker Smart Apex-II CCD diffractometer using graphite-monochromated Mo Kα radiation (λ = 0.71073 Å). Absorption correction was applied by using the multiscan program *SADABS*.[19] The structures were solved by direct methods using SHELXS-97[20] and refined by full-matrix least-squares against F^2 using the SHELXL-97 program[21] or the corresponding programs in the SHELXTL package.[22] H atoms on C and N atoms were placed in calculated positions. Experimental details for the structure analyses of **1**−**4** are given in Table 1. The selected bond distances and angles for **1**−**4** are listed in Table 2.

Results and Discussion

Syntheses and Characterization. A few transition-metal−azido coordination polymers with rigid carboxylate-bearing N-containing heterocycles as coligands have been reported.[13,14] Almost all of these compounds were synthesized by solvothermal methods. Using the same solvothermal technique, compounds **1**−**3** were successfully prepared in our case. Reaction of $MnCl_2$ with NaN_3 and 3,5-diaminobenzoic acid or 4-aminobenzoic acid in a solvent mixture of ethanol and water in an autoclave at 393 K afforded **1** and **3**, respectively, while the reaction of $CdCl_2$ with NaN_3 and 3,5-diaminobenzoic acid under hydrothermal conditions at a temperature of 373 K gave rise to **2**. The successful syntheses in our work, together with those reported previously,[13,14] indicate that the solvothermal reactions are an effective way to obtain azide-based coordination architectures with rigid carboxylate coligands. However, due to the potentially explosive nature of azide, the reactions must be carried out with great care. Compound **4**, which has a flexible amino carboxylic acid coligand, was synthesized using a conventional solution method. Reaction of $Cu(NO_3)_2$ and NaN_3 in the presence of glycine in $H_2O-C_2H_5OH$ at a pH of about 6.4 led to the isolation of **4**. It was found that reactions starting from different cupric salts such as $Cu(NO_3)_2$, $CuCl_2$, and $Cu(ClO_4)_2$ gave the same synthetic result, indicating that the anion of the metal salt does not affect the formation of **4**.

The characteristic ν_{as} stretching vibrations of the N_3^- ion in the IR spectra are observed at 2110 and 2088 cm^{-1} for **1** and 2042 cm^{-1} for **2**, which confirm the EE coordination mode of the N_3^- ion in **1**[23] and the EO coordination mode of the N_3^- ion in **2**.[5] Complex **4** exhibits ν_{as} stretching vibrations at 2111 and 2056 cm^{-1} attributed to the EO coordination mode in **4**, which is similar to $[Cu_2(\mu_2\text{-}1,1\text{-}N_3)_2(NO_3)(Me_3NCH_2CO_2)_2]_n$ with a Cu−N−Cu angle of 119.5(2)° and ν_{as} stretching vibrations at 2101 and 2081 cm^{-1}.[5,24] The strong absorption bands at 2078 cm^{-1} in the IR spectrum of **3** were assigned to the ν_{as} stretching vibration of the N_3^- ion, much broader than those of **1**, **2**, and **4**, indicating a much more complicated coordination mode of the N_3^- ion in **3**. This is consistent with the μ_3-1,1,3- coordination mode in **3** revealed by the single-crystal X-ray diffraction analysis. The strong absorption bands at 1517−1617 and 1379−1413 cm^{-1} can be assigned to the antisymmetric stretching ν_{as} (COO^-) and symmetric stretching ν_s (COO^-) vibrations, respectively, which is consistent with the known complexes.[25] The bands belonging to the amino groups occur in the range of 3450−3150 cm^{-1}.

Crystal Structure of 1. Complex **1** crystallizes in the orthorhombic space group *Pbca* with each Mn(II) in a distorted octahedral geometry completed by two

(19) Sheldrick, G. M. *SADABS*, version 2.05; University of Göttingen: Göttingen, Germany, 2002.
(20) Sheldrick, G. M. *SHELXS-97*, PC Version; University of Göttingen: Göttingen, Germany, 1997.
(21) Sheldrick, G. M. *SHELXL-97*, PC Version; University of Göttingen: Göttingen, Germany, 1997.
(22) Sheldrick, G. M. *SHELXTL NT*, version 5.1; University of Göttingen: Göttingen, Germany, 1997.

(23) Bitschnau, B.; Egger, A.; Escuer, A.; Mautner, F. A.; Sodin, B.; Vicente, R. *Inorg. Chem.* **2006**, *45*, 868–876.
(24) Chow, M. Y.; Zhou, Z. Y.; Mak, T. C. W. *Inorg. Chem.* **1992**, *31*, 4900–4902.
(25) (a) Maji, T. K.; Sain, S.; Mostafa, G.; Lu, T. H.; Ribas, J.; Monfort, M.; Chaudhuri, N. R. *Inorg. Chem.* **2003**, *42*, 709–716. (b) Mondal, K. C.; Sengupta, O.; Nethaji, M.; Mukherjee, P. S. *Dalton Trans.* **2008**, 767–775.

Table 1. Crystal Data and Structure Refinement Parameters for Compounds **1**−**4**

	1	**2**	**3**	**4**
formula	$C_7H_7MnN_5O_2$	$C_7H_7CdN_5O_2$	$C_7H_6MnN_4O_2$	$C_4H_8Cu_2N_8O_4$
fw	248.12	305.58	233.10	359.26
T/K	291(2) K	294(2)	298(2)	298(2)
λ (Mo Kα) (Å)	0.71073	0.71073	0.71073	0.71073
cryst color	brown	brown	brown	green
cryst syst	orthorhombic	monoclinic	monoclinic	orthorhombic
space group	*Pbca*	$P2_1/c$	$P2_1/c$	$Pca2_1$
a, Å	12.6897(9)	8.3972(13)	9.211(4)	14.049(3)
b, Å	8.6978(6)	16.135(2)	11.186(5)	5.7809(14)
c, Å	15.9901(11)	7.0043(11)	8.034(3)	13.021(3)
α, deg	90	90	90	90
β, deg	90	112.921(2)	102.365(5)	90
γ, deg	90	90	90	90
V, Å^3	1764.9(2)	874.1(2)	808.5(6)	1057.5(4)
Z	8	4	4	4
D_c, g cm^{-3}	1.868	2.322	1.915	2.256
μ, mm^{-1}	1.481	2.484	1.607	4.046
F(000)	1000	592	468	712
GOF on F^2	1.043	1.051	1.085	1.060
reflns (collected/unique)	10209/2020	4888/1795	4002/1422	6255/2280
R_{int}	0.0133	0.0260	0.0293	0.0233
R_1[a] ($I > 2\sigma(I)$)	0.0242	0.0232	0.0274	0.0209
wR_2[b] ($I > 2\sigma(I)$)	0.0655	0.0525	0.0583	0.0505
flack Parameter				−0.002(13)

[a] $R_1 = \sum||F_o| - |F_c||/\sum|F_o|$. [b] $wR_2 = [\sum w(F_o^2 - F_c^2)^2/\sum w(F_o^2)^2]^{1/2}$.

carboxylato oxygen atoms from two 3,5-daba ligands, two nitrogen atoms from another two 3,5-daba ligands, and another two nitrogen atoms from two N_3^- ions (Figure 1a). All Mn−O and Mn−N bond lengths fall in the normal range. The O−Mn−N, O−Mn−O, and N−Mn−N bond angles range from 80.14(6) to 168.98(7)°. The N_3^- ligand in **1** adopts a μ-1,3-bridging mode (EE), and the 3,5-daba ligand behaves as a μ_4,η^4- bridge to connect four Mn(II) ions using its two amino groups and one syn−anti carboxylato group. The neighboring Mn(II) ions along the *b* axis are bridged by μ-1,3-N_3^- ions to form a one-dimensional zigzag chain with a Mn···Mn distance of 6.2044(3) Å, as revealed in Figure S1 (Supporting Information). Two neighboring Mn(II) ions from different 1D chains are bridged by two syn−anti carboxylato groups with a Mn···Mn distance of 4.4703(2) Å, resulting in the formation of a two-dimensional network parallel to the *ab* plane, highlighted by purple-colored bonds in Figure 1b. This kind of 2D network is further stabilized by the coordination of one of the amino groups of each 3,5-daba ligand to another Mn(II) ion from another 1D chain within the 2D network. The remaining amino group of each 3,5-daba ligand coordinates to another Mn(II) ion from another 1D chain in the neighboring 2D network, leading to the construction of an overall 3D framework (Figure 1b). Thus, each μ_4,η^4-bridging 3,5-daba ligand interacts with four adjacent 1D zigzag chains via the coordination of two carboxylato oxygen atoms and two amino groups to four Mn(II) ions from the four 1D chains.

As described above, the azide ligand shows a μ-1, 3- bridging mode and connects two Mn(II) ions, while the 3,5-daba ligand coordinates to four Mn atoms, one each per oxygen or nitrogen atom. The Mn(II) ion in turn coordinates to two cis azide ligands and four 3,5-daba ligands. Thus, from a topological viewpoint, the Mn(II) ions act as 6-connecting nodes, and the 3,5-daba ligands act as 4-connecting nodes. The overall 4,6-connected 3D network is shown in Figure S2 (Supporting Information) and has the Schläfli symbol $(4.5^2.6^3)(4.5^9.6^4.7)$.

Crystal Structure of 2. Complex **2** crystallizes in the monoclinic space group $P2_1/c$. The Cd(II) ion in **2** presents a distorted octahedral geometry with coordination of two carboxlato oxygen atoms from two 3,5-daba ligands, two nitrogen atoms from another two 3,5-daba ligands, and another two nitrogen atoms from two N_3^- ions (Figure 2a), which is similar to the Mn(II) ion of **1**. The Cd−O and Cd−N bond lengths are in a normal range of 2.300(2)−2.412(2) Å and 2.364(3)−2.429(3) Å, respectively. The O−Cd−N, O−Cd−O, and N−Cd−N bond angles range from 76.23(9) to 163.23(9)°. The 3,5-daba ligand in **2** adopts the same μ_4,η^4-bridging mode as that in **1**, connecting four Cd(II) ions using its two amino groups and one syn−anti carboxlato group. This is very different from the reported 2D Cd(II)−3,5-daba complexes, in which 3,5-daba acts as tridentate or bidentate ligand.[26] Although the 3,5-daba ligands in **1** and **2** present the same bridging mode, the N_3^- ligand in **2** shows a μ-1,1-bridging mode (EO) which is different from the μ-1,3-bridging mode (EO) in **1**.

Every two adjacent Cd(II) ions in **2** are connected by one μ-1,1-N_3^- ligand and one syn−anti carboxyla to group forming a one-dimensional chain parallel to the *c* axis (Figure S3, Supporting Information) with a Cd···Cd separation of 3.9118(5) Å and a Cd−N−Cd angle of 108.239(2)°. The further coordination of the two amino groups of each 3,5-daba ligand in one 1D chain to two Cd(II) ions from another two adjacent 1D chains leads to the connection of each 1D chain to six adjacent chains. Thus, each 3,5-daba ligand in **2** links just three 1D chains, which are different from that in **1**. The propagation of this kind of connection results in the construction of a 3D metal−organic framework, as shown in Figure 2b.

(26) Ye, Q.; Chen, X.-B.; Song, Y.-M.; Wang, X.-S.; Zhang, J.; Xiong, R.-G.; Fun, H.-K.; You, X.-Z. *Inorg. Chim. Acta* **2005**, *358*, 1258–1262.

Table 2. Selected Bond Lengths (Å) and Angles (deg) for **1**−**4**[a]

			1		
Mn1−O2A	2.1395(12)	Mn1−N5B	2.1840(17)	Mn1−N2C	2.3113(13)
Mn1−O1	2.1422(11)	Mn1−N3	2.2386(18)	Mn1−N1D	2.3646(13)
O2A−Mn1−O1	111.45(5)	N5B−Mn1−N3	97.91(10)	O2A−Mn1−N1D	166.25(5)
O2A−Mn1−N5B	88.69(7)	O2A−Mn1−N2C	81.44(6)	O1−Mn1−N1D	81.56(5)
O1−Mn1−N5B	91.73(6)	O1−Mn1−N2C	87.38(5)	N5B−Mn1−N1D	95.56(7)
O2A−Mn1−N3	86.33(6)	N5B−Mn1−N2C	168.98(7)	N3−Mn1−N1D	80.14(6)
O1−Mn1−N3	160.04(8)	N3−Mn1−N2C	86.39(9)	N2C−Mn1−N1D	95.17(4)
			2		
Cd1−O1	2.300(2)	Cd1−N3B	2.399(3)	Cd1−O2B	2.412(2)
Cd1−N1A	2.364(3)	Cd1−N2C	2.410(3)	Cd1−N3	2.429(3)
O1−Cd1−N1A	76.23(9)	N3B−Cd1−N2C	87.87(9)	O1−Cd1−N3	114.78(9)
O1−Cd1−N3B	90.69(9)	O1−Cd1−O2B	81.93(8)	N1A−Cd1−N3	98.87(9)
N1A−Cd1−N3B	160.88(9)	N1A−Cd1−O2B	86.13(9)	N3B−Cd1−N3	99.28(9)
O1−Cd1−N2C	151.24(9)	N3B−Cd1−O2B	78.16(9)	N2C−Cd1−N3	93.78(9)
N1A−Cd1−N2C	96.90(9)	N2C−Cd1−O2B	69.66(9)	O2B−Cd1−N3	163.23(9)
			3		
Mn1−O1	2.097(2)	Mn1−N2B	2.255(2)	Mn1−N1D	2.314(2)
Mn1−O2A	2.109(2)	Mn1−N4C	2.259(2)	Mn1−N2	2.346(2)
O1−Mn1−O2A	94.99(9)	N2B−Mn1−N4C	97.41(8)	O1−Mn1−N2	85.60(8)
O1−Mn1−N2B	165.19(8)	O1−Mn1−N1D	86.70(9)	O2A−Mn1−N2	92.03(8)
O2A−Mn1−N2B	89.12(9)	O2A−Mn1−N1D	177.94(9)	N2B−Mn1−N2	80.03(8)
O1−Mn1−N4C	96.67(8)	N2B−Mn1−N1D	88.95(9)	N4C−Mn1−N2	175.27(8)
O2A−Mn1−N4C	91.90(8)	N4C−Mn1−N1D	89.06(9)	N1D−Mn1−N2	86.93(8)
			4		
Cu1−O1	1.959(2)	Cu1−O4A	2.321(2)	Cu2−N3	2.001(2)
Cu1−N6	1.988(2)	Cu2−O3	1.9663(19)	Cu2−N6B	2.020(2)
Cu1−N1	1.998(3)	Cu2−N2	1.966(3)	Cu2−O2C	2.328(2)
Cu1−N3	2.016(2)	O1−Cu1−O4A	104.62(9)	N3−Cu2−N6B	93.43(10)
O1−Cu1−N6	84.76(9)	N6−Cu1−O4A	101.96(10)	O3−Cu2−O2C	97.23(8)
O1−Cu1−N1	83.89(9)	N3−Cu1−O4A	89.02(8)	N2−Cu2−O2C	92.24(14)
N6−Cu1−N1	167.43(10)	O3−Cu2−N2	83.73(10)	N3−Cu2−O2C	98.12(9)
O1−Cu1−N3	166.25(8)	O3−Cu2−N3	86.71(8)	N6B−Cu2−O2C	86.81(8)
N6−Cu1−N3	94.19(10)	N2−Cu2−N3	166.70(14)	Cu2−N3−Cu1	117.29(10)
N1−Cu1−N3	95.55(10)	O3−Cu2−N6B	175.89(9)	Cu1−N6−Cu2D	116.85(11)
N1−Cu1−O4A	86.14(10)	N2−Cu2−N6B	95.46(11)		

[a] Symmetry codes. For **1**: (A) $-x+1, -y+1, -z+1$; (B) $-x+1/2, y+1/2, z$; (C) $-x+3/2, y-1/2, z$; (D) $x-1/2, y, -z+3/2$; (E) $x+1/2, y, -z+3/2$; (F) $-x+3/2, y+1/2, z$; (G) $-x+1/2, y-1/2, z$. For **2**: (A) $-x, y-1/2, -z+3/2$; (B) $x, -y+3/2, z-1/2$; (C) $x-1, -y+3/2, z-1/2$. For **3**: (A) $x, -y+1.5, z+0.5$; (B) $-x+1, -y+2, -z+1$; (C) $-x+1, y-0.5, -z+0.5$; (D) $x-1, y, z$. For **4**: (A) $x-1/2, -y+2, z$; (B) $x, y-1, z$; (C) $-x+1, -y+2$.

The structure analysis reveals that the structure of **2** is similar to that of **1** in that it contains one unique metal ion, one unique N_3^- anion, and one unique 3,5-daba ligand. However, while the bridging azide again bridges two metals, this time it shows the shorter μ-1,1-bridging mode. As before, the 3,5-daba ligand connects four metals, and the metals coordinate to two cis azide ligands and four 3,5-daba ligands. Thus, a 3D 4,6-connected network is again formed (Figure S4, Supporting Information); however, the topology is different from that seen in **1**. The Schläfli symbol is $(3.4^2.5^3)(3^2.4^2.5^4.6^5.7^2)$.

Crystal Structure of 3. As shown in Figure 3a, the asymmetric unit of **3** consists of one unique Mn(II) ion, one unique 4-aba, and one unique N_3^- ion. The Mn(II) ion of **3** is six-coordinated in a distorted octahedral geometry by two carboxylato oxygen atoms from two 4-aba ligands, one amino group from another 4-aba ligand, and three nitrogen atoms from three N_3^- ions. The Mn−O and Mn−N bond lengths of **3** are in the ranges of 2.097(2)−2.109(2) and 2.255(2)−2.346(2), respectively, which are comparable to those in **1** and the reported cases.[27] The O−Mn−N, O−Mn−O, and N−Mn−N bond angles of **3** range from 80.03(8) to 177.94(9)°. The 4-aba ligand of **3** acts as a μ_3,η^3-bridge to connect three Mn(II) ions using its amino group and the syn−anti carboxylato group. The N_3^- ligand in **3** adopts a μ_3-1,1,3-bridging mode connecting three Mn(II) ions together, which is different from the μ-1,3 and μ-1,1 bridging modes in **1** and **2**.

Two Mn(II) ions of **3** are bridged by two N_3^- ligands in a μ-1,1-bridging mode generating a dinuclear building block with a Mn···Mn distance of 3.5244(11) Å. Each dinuclear building block provides the two nitrogen atoms at the other end of the two N_3^- ligands to coordinate to

(27) (a) Chen, Z.; Ma, Y.; Liang, F.; Zhou, Z. *J. Organomet. Chem.* **2008**, *693*, 646–654. (b) Durot, S.; Policar, C.; Pelosi, G.; Bisceglie, F.; Mallah, T.; Mahy, J. P. *Inorg. Chem.* **2003**, *42*, 8072–8080. (c) Yao, Y. L.; Che, Y. X.; Zheng, J. M. *Cryst. Growth Des.* **2008**, *8*, 2299–2306. (d) Ma, C. B.; Chen, C. N.; Liu, Q. T.; Chen, F.; Liao, D. Z.; Li, L. C.; Sun, L. C. *Eur. J. Inorg. Chem.* **2003**, 2872–2879.

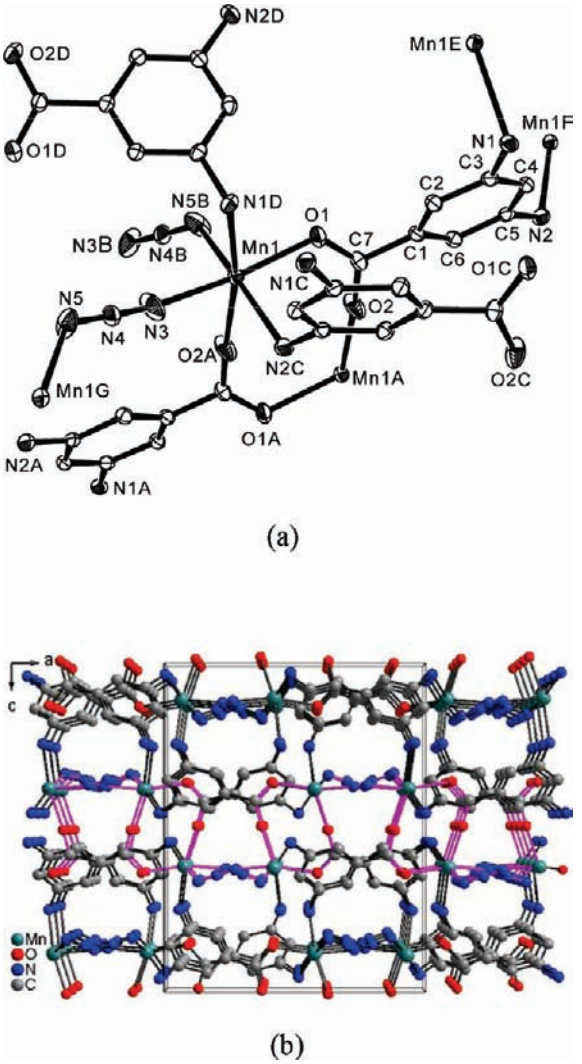

Figure 1. (a) A view of the coordination environment of the Mn(II) ion and the binding fashions of 3,5-daba and N_3^- ligands in **1** with displacement ellipsoids drawn at the 30% probability level. Symmetry codes: (A) $-x + 1, -y + 1, -z + 1$; (B) $-x + 1/2, y + 1/2, z$; (C) $-x + 3/2, y - 1/2, z$; (D) $x - 1/2, y, -z + 3/2$; (E) $x + 1/2, y, -z + 3/2$; (F) $-x + 3/2, y + 1/2, z$; (G) $-x + 1/2, y - 1/2, z$. (b) A view of the 3D framework of **1** showing a 2D network highlighted by purple-colored bonds. Hydrogen atoms are omitted for clarity.

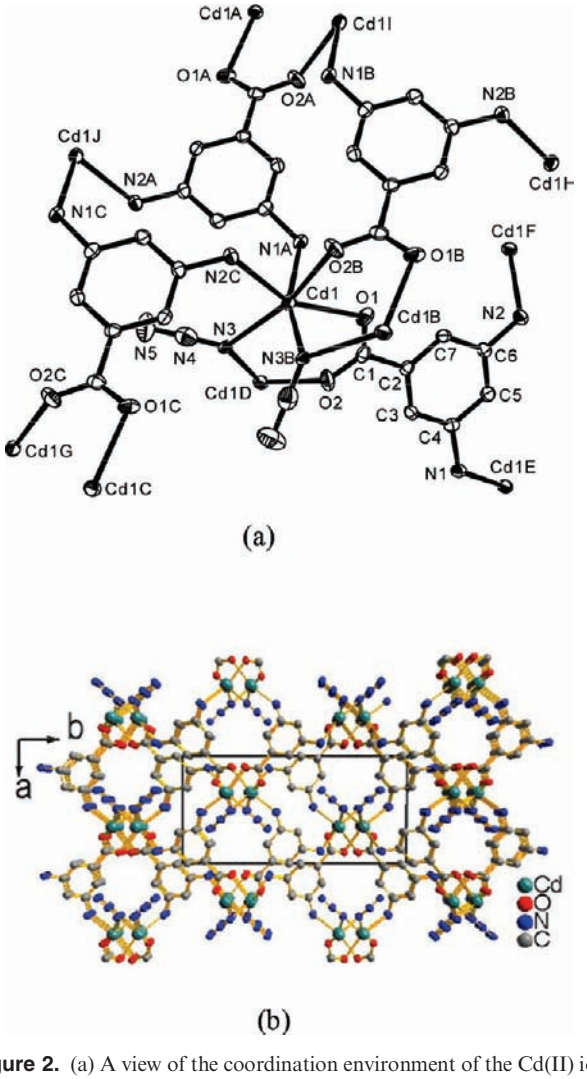

Figure 2. (a) A view of the coordination environment of the Cd(II) ion and the binding fashions of 3,5-daba and N_3^- ligands in **2** with displacement ellipsoids drawn at the 30% probability level. Symmetry codes: (A) $-x, y - 1/2, -z + 3/2$; (B) $x, -y + 3/2, z - 1/2$; (C) $x - 1, -y + 3/2, z - 1/2$; (D) $x, -y + 3/2, z + 1/2$; (E) $-x, y + 1/2, -z + 3/2$; (F) $x + 1, -y + 3/2, z + 1/2$; (G) $-1 + x, y, z$, (H) $x + 1, y, z$, (I) $-x, 1 - y, 1 - z$, (J) $-1 - x, 1 - y, 1 - z$. (b) A view of the 3D metal-organic framework of **2**. Hydrogen atoms are omitted for clarity.

two Mn(II) ions from another two dinuclear building blocks, with Mn···Mn distances of 4.8793(15) and 5.9164(12) Å. Thus, the N_3^- ligands display a 3-connecting μ_3-1,1,3-bridging mode and join the metal atoms into 2D (4.8^2) sheets parallel to the *bc* plane (Figure 3b) with the 4-aminophenyl groups aligned on both sides of the 2D plane alternatively. These sheets are reinforced by syn−anti carboxylate bridges from the 4-aba ligands via connecting the nearest two Mn(II) ions from two adjacent dinuclear building blocks. Ultimately, the 4-aba ligands connect the 2D sheets into a 3D network through the coordination of the amino groups to the Mn(II) ions from adjacent 2D sheets, and vice versa, as shown in Figure S5 (Supporting Information).

Topologically, the structure is composed of 3-connecting azide anions, 3-connecting 4-aba ligands, and 6-connecting Mn atoms. The complicated trinodal 3,6-connected network is shown in Figure 4 and Figure S6 (Supporting Information). To the best of our knowledge, this 3,6-connected net has not been reported.[28] It has the Schläfli symbol $(4^2.6)(4.6^2)(4^3.6^6.8^6)$.

Crystal Structure of 4. The structure of **4** contains two unique Cu atoms, two unique azide anions, and two unique gly ligands in one asymmetric unit, as revealed in Figure 5a. Chemically, however, each pair shows the same coordination environment. Each Cu(II) ion coordinates to one gly ligand, which chelates via its nitrogen atom and one oxygen atom, coordinates to another gly ligand in a monodentate fashion via one oxygen atom, and coordinates to two nitrogen atoms from two μ-1,1 bridging azide anions, forming a distorted square-pyramidal geometry. Both the N_3^- and gly ligands of **4** in turn connect pairs of Cu(II) ions via μ-1,1- and μ_2, η^3-bridging coordination modes, respectively. Cu(II) ions are bridged by μ-1,1-bridging N_3^- to form one-dimensional zigzag chains along the *b* axis (Figure 5b)

(28) Du, M.; Zhang, Z.-H.; Tang, L.-F.; Wang, X.-G.; Zhao, X.-J.; Batten, S. R. *Chem.—Eur. J.* **2007**, *13*, 2578–2586.

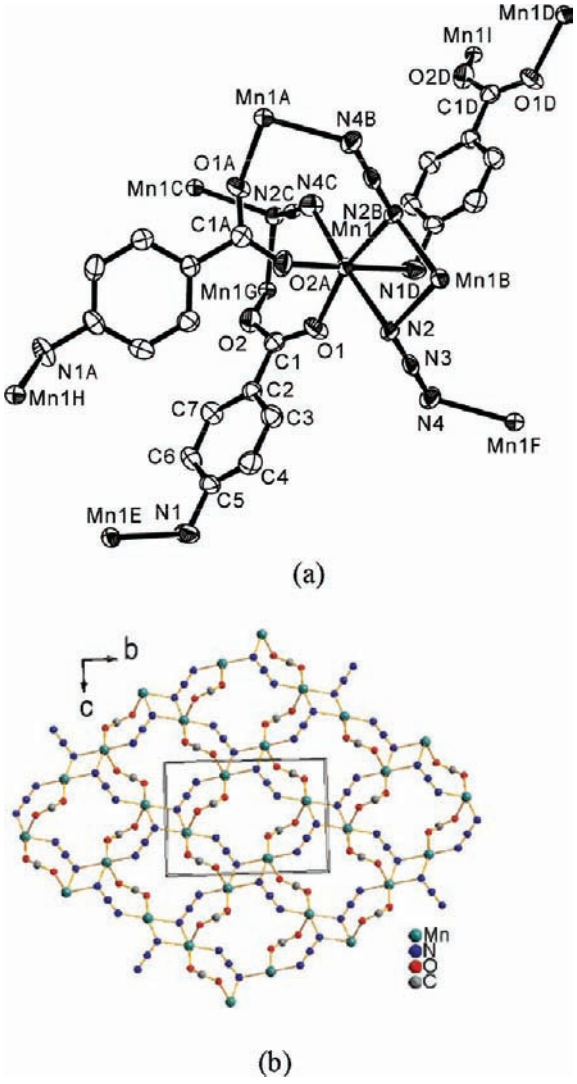

Figure 3. (a) A view of the coordination environment of the Mn(II) ion and the binding fashions of the 4-aba and N_3^- ligands in **3** with displacement ellipsoids drawn at the 30% probability level. Symmetry codes: (A) $x, -y + 1.5, z + 0.5$; (B) $-x + 1, -y + 2, -z + 1$; (C) $-x + 1, y - 0.5, -z + 0.5$; (D) $x - 1, y, z$; (E) $x + 1, y, z$; (F) $-x + 1, y + 0.5, -z + 0.5$; (G) $x, -y + 1.5, z - 0.5$; (H) $x + 1, -y + 1.5, z + 0.5$; (I) $x - 1, -y + 1.5, z - 0.5$. (b) The 2D sheet in **3** constructed by Mn(II) ions, N_3^- anions, and the carboxlato groups of 4-aba ligands with 4-aminophenyl groups omitted for clarity.

with a Cu···Cu distance of 3.4145(6) Å and a Cu−N−Cu angle of 116.851(8)°. Each 1D chain is then linked to four other 1D chains by the μ_2,η^3-bridging gly ligands via the coordination of the amino group and one carboxylato oxygen atom to one Cu(II) ion from one 1D chain and the other oxygen atom to another Cu(II) ion in an adjacent chain. This means the carboxylato group of the gly ligand acts as an anti−anti bridge connecting Cu(II) ions from adjacent 1D chains with a Cu···Cu distance of 6.0532(12) Å. Thus, a 3D framework is constructed as shown in Figure 5d. Alternatively, one can say that the neighboring Cu(II) ions are connected by μ_2,η^3-bridging gly ligands to form one-dimensional chains (Figure 5c) running along the *c* axis, which are further bridged by the μ-1,1-bridging N_3^- ions into the three-dimensional framework. Therefore, there exist two kinds of chains in **4**: −Cu−anti−anti−COO^-−Cu− running along the *c* axis and −Cu−EO−N_3^-−Cu− running along the *b* axis.

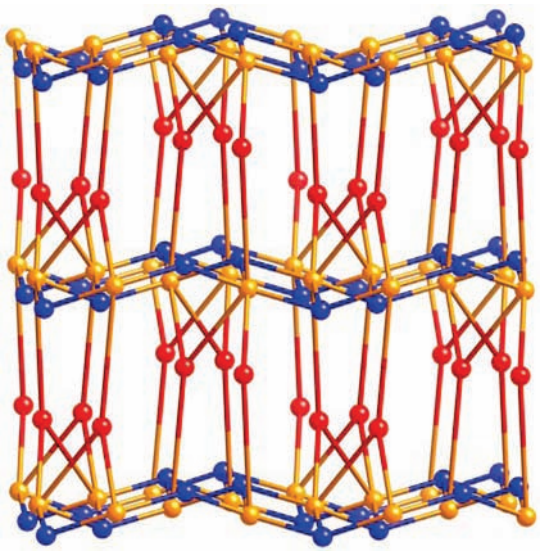

Figure 4. The overall network topology of **3**, viewed side-on to the layers shown in Figure 3b. Orange spheres represent the Mn nodes. Blue spheres represent the azide anions, and red spheres represent the 4-aba ligands.

Topologically, the Cu(II) ions in the 3D framework of **4** act as 4-connecting nodes, while the ligands all act as simple bridges between the metal atoms. The 4-connected 3D net formed is shown in Figure 6; it has the Lonsdaleite (hexagonal diamond) topology. This is very unusual; there are only a few reports of coordination polymers with this topology,[29] despite its simplicity—tetrahedral nodes more usually form networks with the cubic diamond topology.[30]

Magnetic Properties of 1, 3, and 4. The magnetic properties of **1** and **3** were investigated by solid-state magnetic susceptibility (χ_m) measurements in the 2.0−300 K range in a DC field of 10 000 Oe. The magnetic properties of complexes **1** and **3** in the form of both $\chi_M T$ and χ_M versus T plots are shown in Figures 7 and 8, respectively. The values of $\chi_M T$ at 300 K are 4.0049 and 3.6176 cm^3 K mol^{-1} for **1** and **3**, respectively, both of which are lower than that expected (4.38 cm^3 K mol^{-1}) for one magnetically isolated high-spin Mn(II) ion. Decreasing the temperature leads to the $\chi_m T$ values of **1** and **3** gradually decreasing, reaching 0.1647 and 0.05562 cm^3 K mol^{-1} at 2.0 K for **1** and **3**, respectively. These features are typical of a significant antiferromagnetic coupling in **1** and **3**. The χ_m values of **1** and **3** rise sharply to reach a maximum of 0.08037 cm^3 mol^{-1} at 14 K for **1** and 0.03014 cm^3 mol^{-1} at 50.4 K for **3**, then decrease rapidly to 0.07853 cm^3 mol^{-1} at 8.1 K for **1** and 0.02685 cm^3 mol^{-1} at 11.1 K for **3**, and finally rise sharply again to 0.08236 and 0.02774 cm^3 mol^{-1} for **1** and **3** at 2 K, respectively. The characteristics of χ_m in the low-temperature range for both **1** and **3** might be attributed to the presence of trace of paramagnetic impurities.[31]

(29) (a) Sreenivasulu, B.; Vittal, J. J. *Cryst. Growth Des.* **2003**, *3*, 635–637. (b) Kitazawa, T.; Kikuyama, T.; Takeda, M.; Iwamoto, T. *J. Chem. Soc., Dalton Trans.* **1995**, 3715–3720.
(30) Batten, S. R. *J. Solid State Chem.* **2005**, *178*, 2475–2479.
(31) (a) Gao, E. Q.; Cheng, A. L.; Xu, Y. X.; He, M. Y.; Yan, C. H. *Inorg. Chem.* **2005**, *44*, 8822–8835. (b) Thétiot, F.; Triki, S.; Pala, J. S.; Galán-Mascarós, J. R.; Martínez-Agudo, J. M.; Dunbar, K. R. *Eur. J. Inorg. Chem.* **2004**, 3783–3791. (c) Zhao, W.; Song, Y.; Okamura, T. A.; Fan, J.; Sun, W. Y.; Ueyama, N. *Inorg. Chem.* **2005**, *44*, 3330–3336.

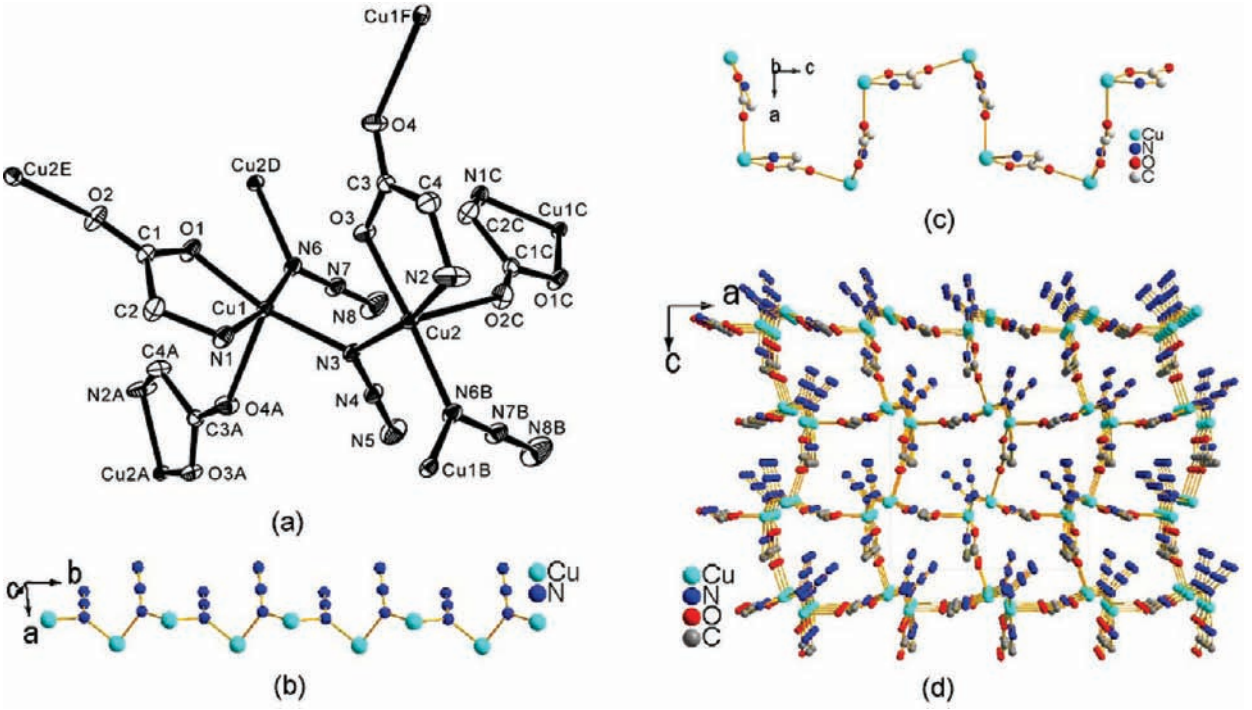

Figure 5. (a) A view of the coordination environment of the Cu(II) ion and the binding fashions of the gly and N_3^- ligands in **4** with displacement ellipsoids drawn at the 30% probability level. Symmetry codes: (A) $x-1/2, -y+2, z$; (B) $x, y-1, z$; (C) $-x+1, -y+2, z-1/2$; (D) $x, y+1, z$; (E) $-x+1, -y+2, z+1/2$; (F) $x+1/2, -y+2, z$. (b) The 1D chain in **4** constructed by Cu(II) ions and N_3^- anions. (c) The 1D chain in **4** constructed by Cu(II) ions and gly anions. (d) A view of the 3D metal-organic framework of **4**. Hydrogen atoms are omitted for clarity.

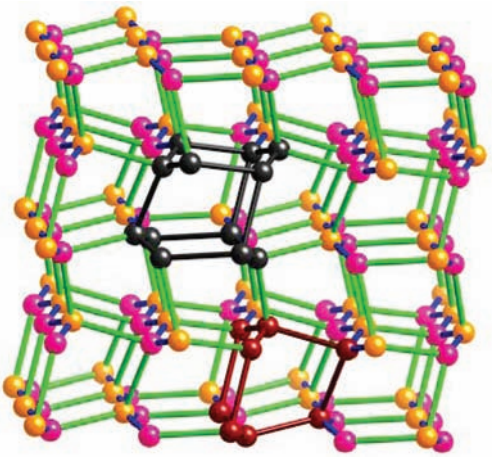

Figure 6. The unusual Lonsdaleite topology of **4**. Spheres represent the two different Cu nodes, although topologically both nodes are equivalent. The two types of cavities in the Lonsdaleite net are highlighted. Green bonds represent the gly bridges, while blue bonds represent the azide bridges.

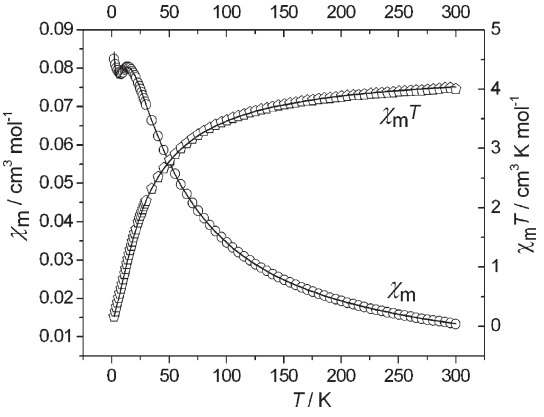

Figure 7. Plots of χ_m and $\chi_m T$ vs T for **1**. Solid lines show the best fit of the data according to the proposed model.

Fitting of the $\chi_m^{-1} - T$ above 100 K using the Curie–Weiss law $\chi_m = C/(T-\theta)$ gives the Curie constants $C = 4.35$ and 4.65 cm^3 K mol^{-1} and the Weiss constants $\theta = -24.59$ and -84.07 K for **1** and **3**, respectively. The negative θ values also support the presence of overall antiferromagnetic interactions in the two complexes.

Magnetically, **1** presents a 2D network because the Mn(II) ions from neighboring 2D sheets are bridged by 3,5-daba via the coordination of its two amino groups, which do not transmit magnetic exchange effectively. There are two types of Mn(II)–Mn(II) magnetic exchange interactions in the 2D network of **1**. Type 1 is through a bridging end-to-end N_3^- ion between the manganese(II) centers, which creates an infinite $-Mn-N_3-Mn-$ chain, and is treated as the intrachain interaction. Type 2 is through a double carboxylato bridge of two 3,5-daba ligands between the Mn(II) ions from adjacent chains, which is taken as the interchain interaction. Similar to the case of **1**, **3** also exhibits a 2D sheet from the point of view of magnetic exchange as the bridge of 4-aba between the adjacent 2D sheets cannot effectively transmit magnetic exchange. Every two adjacent Mn(II) ions in the chain along the c axis transmit the magnetic exchange through the bridges of one syn–anti carboxylato group and one end-to-end N_3^- ion simultaneously. The interchain magnetic exchange is performed by double end-on N_3^- ions. Thus, the experimental magnetic behavior of **1** and **3** can be simulated using the analytical expression derived by Fisher for a 1D

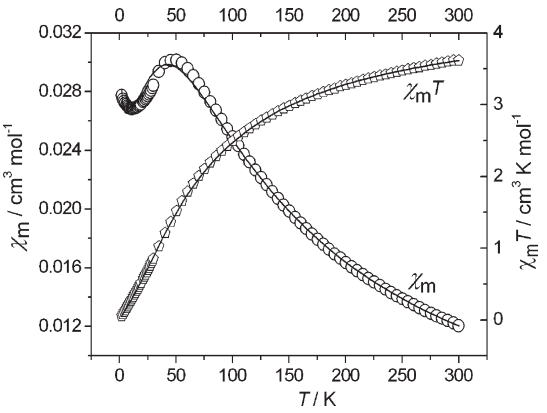

Figure 8. Plots of χ_m and $\chi_m T$ vs T for **3**. Solid lines show the best fit of the data according to the proposed model.

Heisenberg chain of classical spins ($S = 5/2$, $H = -J\Sigma_i\Sigma_{i+1}$)[32] with a consideration of interchain magnetic exchange estimated by the mean field model:

$$\chi_{chain} = \frac{Ng^2\beta^2S(S+1)(1+u)}{3kT(1-u)}$$

$$\chi_{2D} = \frac{\chi_{chain}}{1-(2zJ'/Ng^2\beta^2)\chi_{chain}}$$

where N is Avogadro's number, β is Bohr's magneton, k is Boltzmann's constant, and u is the Langevin function: $u = \coth[JS(S+1)/kT] - kT/[JS(S+1)]$.

The low-temperature increase of χ_m in antiferromagnetic systems is usually attributed to the presence of a certain amount of paramagnetic impurities.[31] Following this line, we simulated the experimental data of **1** and **3** to the following equation over the whole 2−300 K temperature range:

$$\chi_m = \chi_{2D}(1-\rho) + [Ng^2\beta^2S(S+1)/3kT]\rho$$

where ρ is the amount of the paramagnetic impurities [presumably a mononuclear Mn(II) complex]. The best least-squares fit of the theoretical equation to experimental data leads to $g = 2$, $J = -2.50(1)$ cm^{-1}, $zJ' = -0.42(4)$ cm^{-1}, and $\rho = 0.76\%$ with an agreement factor of $R = 8.06 \times 10^{-5}$ for **1** and $g = 2$, $J = -7.14(1)$ cm^{-1}, $zJ' = 0.22(3)$ cm^{-1}, and $\rho = 0.15\%$ with an agreement factor of $R = 3.51 \times 10^{-4}$ for **3**. These values again indicate the presence of dominant weak antiferromagnetic interaction between the neighboring Mn(II) ions in both **1** and **3**. The intrachain J ($J = -2.50(1)$ cm^{-1}) and interchain J ($zJ' = -0.42(4)$ cm^{-1}) of **1** are ascribed to the EE-azido and double *syn*−*anti*-carboxylato bridges, respectively, which usually lead to antiferromagnetic interactions. With the fitting model in mind, the J value of −7.14(1) cm^{-1} for **3** is attributed to the bridges of one syn−anti carboxyla to group and one end-to-end N_3^- ion. The interchain J ($zJ' = 0.22(3)$ cm^{-1}) of **3** corresponds to the magnetic coupling mediated by the double EO-azido bridges, which confirms that the EO-azido bridge in **3** mediates a ferromagnetic interaction between the neighboring Mn(II) ions. It might be caused by the small Mn−$N_{EO\text{-}azido}$−Mn angle (99.97(8)°), which is consistent with the related cases reported[33,34] and confirms again the conclusion that one of the driving effects for magnetic interactions through the EO-azido bridge in Mn(II) compounds seems to be the value of the bridging angle of Mn−$N_{EO\text{-}azido}$−Mn.[4,34]

The magnetic properties of **4** were investigated by solid-state magnetic susceptibility (χ_m) measurements in the 1.8−300 K range in a DC field of 2000 Oe. The magnetic properties of complex **4** in the form of both $\chi_M T$ and χ_M versus T plots are shown in Figure 9. The $\chi_m T$ value of **4** at 300 K is 1.1290 cm^3 K mol^{-1}, which is higher than that (0.75 cm^3 K mol^{-1}) expected for two magnetically isolated high-spin Cu^{II} ions. With the decrease of temperature, the $\chi_m T$ values increase slowly, and below 50 K, they rise up more quickly to reach a maximum of 5.65 cm^3 K mol^{-1} at 7.0 K. This behavior indicates the occurrence of a relative strong ferromagnetic coupling in **4**. On further cooling, they decrease sharply to 1.10 cm^3 K mol^{-1} at 1.8 K (Figure 9). Fitting the data to the Curie−Weiss law $\chi_m = C/(T-\theta)$ above 100 K, as show in Figure S7 (Supporting Information), gives a Curie constant of 1.01 cm^3 K mol^{-1} and a positive Weiss constant of 31.34 K, which suggest the presence of dominant ferromagnetic coupling in **4**. Considering its structure, there are two sets of magnetic exchange pathways. One consists of one EO azido bridge, and the other consists of one anti−anti carboxylato bridge. It has been shown previously that the EO azido bridge in basal−basal dispositions favors an antiferromagnetic interaction when the Cu−N−Cu angle is larger than 104° from density functional calculations[4] or 108.5° from an experimental study.[5] The Cu−N−Cu angles in our case of **4** are 116.85(11) and 117.29(1)°, which indicates an occurrence of antiferromagnetic coupling through the EO azido bridge in **4**. The anti−anti carboxylato group in the case of **4** connects two Cu(II) ions through the axial−equatorial pathway with a dihedral angle of 70.194° between the mean equatorial planes of adjacent copper atoms. According to the reported cases, this kind of *anti*−*anti*-carboxylato bridge in Cu(II) complexes usually mediates a ferromagnetic interaction between Cu^{II} ions.[35]

(32) Kahn, O. *Molecular Magnetism*; VCH: New York, 1993; p 258. Fisher, M. E. Am. J. Phys. 1964, 32, 343.

(33) (a) Zhang, H. Y.; Liu, C. M.; Zhang, D. Q.; Gao, S.; Zhu, D. B. *Inorg. Chem. Commun.* **2007**, *10*, 897–901. (b) Gao, E. Q.; Bai, S. Q.; Yue, Y. F.; Wang, Z. M.; Yan, C. H. *Inorg. Chem.* **2003**, *42*, 3642–3649. (d) Abu-Youssef, M. A. M.; Escuer, A.; Gatteschi, D.; Goher, M. A. S.; Mautner, F. A.; Vicente, R. *Inorg. Chem.* **1999**, *38*, 5716–5723. (e) Villanueva, M.; Mesa, J. L.; Urtiaga, M. K.; Cortés, R.; Lezama, L.; Arriortua, M. I.; Rojo, T. *Eur. J. Inorg. Chem.* **2001**, 1581–1586. (f) Abu-Youssef, M. A. M.; Escuer, A.; Goher, M. A. S.; Mautner, F. A.; Vicente, R. *Eur. J. Inorg. Chem.* **1999** 687–691.

(34) (a) Tang, L. F.; Zhang, L.; Li, L. C.; Cheng, P.; Wang, Z. H.; Wang, J. T. *Inorg. Chem.* **1999**, *38*, 6326–6328. (b) Cortés, R.; Drillon, M.; Solans, X.; Lezama, L.; Rojo, T. *Inorg. Chem.* **1997**, *36*, 677–683.

(35) (a) Colacio, E.; Domínguez-Vera, J. M.; Ghazi, M.; Kivekäs, R.; Klinga, M.; Moreno, J. M. *Eur. J. Inorg. Chem.* **1999**, 441–445. (b) Delgado, F. S.; Ruiz-Pérez, C.; Sanchiz, J.; Lloret, F.; Julve, M. *CrystEngComm* **2006**, *8*, 507–529. (c) Delgado, F. S.; Ruiz-Pérez, C.; Sanchiz, J.; Lloret, F.; Julve, M. *CrystEngComm* **2006**, *8*, 530–544. (d) Pasán, J.; Delgado, F. S.; Rodriguez-Martín, Y.; Hernández-Molina, M.; Ruiz-Pérez, C.; Sanchiz, J.; Lloret, F.; Julve, M. *Polyhedron* **2003**, *22*, 2143–2153. (e) Sanchiz, J.; Rodríguez-Martín, Y.; Ruiz-Pérez, C.; Mederos, A.; Lloret, F.; Julve, M. *New J. Chem.* **2002**, *26*, 1624–1628. (f) Yang, C. T.; Moubaraki, B.; Murray, K. S.; Vittal, J. J. *Dalton Trans.* **2003**, 880–889.

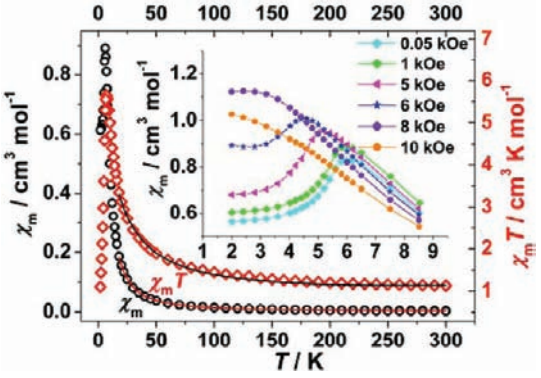

Figure 9. Plots of χ_m and $\chi_m T$ vs T for **4** measured in an applied field of 2 kOe. The solid lines represent the theoretical fits in the high-temperature region (see text). Inset: Plots of χ_m vs T measured between 2.00 and 8.5 K at the indicated applied fields (solid lines are a guide for the eye).

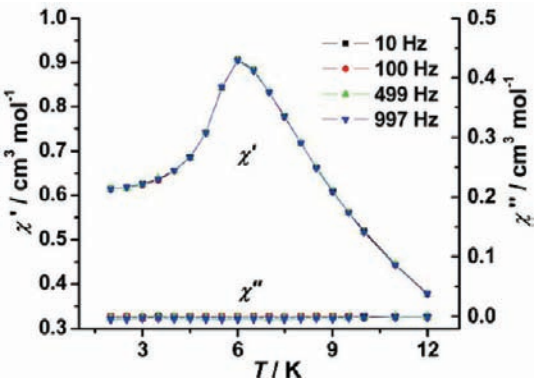

Figure 10. Temperature-dependent ac magnetic susceptibilities of **4** under different frequencies (10, 100, 499, and 997 Hz) with a zero DC field and an oscillating field of 2.5 Oe. Solid lines are guides for the eye.

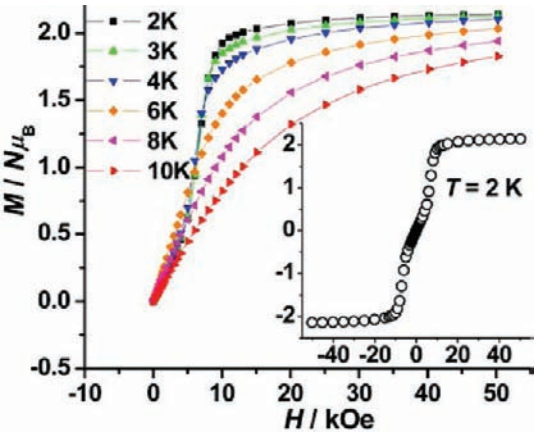

Figure 11. Field dependence of the magnetization at different temperatures and below 50 kOe for **4**. Inset: The whole field dependence of the magnetization between −50 and +50 kOe, emphasizing the absence of a hysteresis effect.

The magnetic susceptibility data revealed that the ferromagnetic coupling is relatively strong and the antiferromagnetic coupling is relatively weak. According to the structural analysis, compound **4** would be three-dimensional, with a large ferromagnetic coupling (J) mediated by the *anti*−*anti*-carboxylato bridge within the −Cu−*anti*−*anti*-COO$^-$−Cu− chain and a weak antiferromagnetic coupling mediated by the EO azido bridge within the −Cu−EO−N$_3^-$−Cu− chain. The weak antiferromagnetic coupling mediated by the EO azido bridge can also be understood as an interchain coupling (zJ') between the neighboring −Cu−*anti*−*anti*-COO$^-$−Cu− chains. Consequently, the experimental magnetic behavior of **4** can be simulated using the expression proposed by Baker et al. for a Heisenberg ferromagnetic $S = 1/2$ chain based on the Hamiltonian $H = -J\Sigma S_i S_{i+1}$[36] with a consideration of interchain magnetic exchange estimated by mean field model:

$$\chi_{chain} = \frac{Ng^2\beta^2}{4kT}\left(\frac{A}{B}\right)^{2/3}$$

where $A = 1.0 + 5.7979916x + 16.902653x^2 + 29.376885x^3 + 29.832959x^4 + 14.036918x^5$, $B = 1.0 + 2.7979916x + 7.0086780x^2 + 8.6538644x^3 + 4.5743114x^4$, and $x = J/2kT$.

$$\chi_{3D} = \frac{\chi_{chain}}{1-(2zJ'/Ng^2\beta^2)\chi_{chain}}$$

The best fit for **4** in the temperature range of 18−300 K as shown in Figure 9 gives $J = 149(1)$ cm^{-1}, $g = 2.29(1)$, and $zJ' = -0.23(2)$ cm^{-1} with an agreement factor of $R = 1.91 \times 10^{-4}$. These coupling constants clearly confirm that the *anti*−*anti*-carboxylato bridge mediates a strong ferromagnetic interaction and the EO azido bridge favors a weak antiferromagnetic interaction in **4**.

Further magnetic investigation reveals that **4** is a metamagnet. The field-cooled magnetizations under different fields are shown in the inset of Figure 9. At a low field, the χ_m versus T curves all display a maximum, suggesting the occurrence of 3D antiferromagnetic ordering in **4**. Upon increasing the field, the maximum moved to lower temperatures and became less prominent and finally disappeared at an applied field of 8 and 10 kOe, indicating that the interchain antiferromagnetic interactions are overcome by the external field. These features are characteristic of metamagnetic behaviors. To confirm the appearance of magnetic transition and to determine the critical temperature, the ac susceptibilities (in phase χ' and out-of-phase χ'') measured as a function of temperature in the low-temperature range were obtained by a 2.5 Oe ac field oscillating at 10, 100, 499, and 997 Hz under a zero DC field as shown in Figure 10. The in-phase part, χ', of all of the frequencies exhibits a frequency-independent maximum value at 6 K (T_N). The ZFCMs and FCMs at 100 Oe reveal no divergence, as shown in Figure S8 (Supporting Information).

The metamagnetic behavior of **4** is also confirmed by the field-dependent magnetization measured at different temperatures, as depicted in Figure 11. The curves measured at 2, 3, and 4 K, which are below critical temperature, present a pronounced sigmoid shape. The magnetization measured at 4 K increases linearly below 4 kOe, then more quickly below 10 kOe. At last, it rises very slowly, reaching a saturation value of ca. 2.10 $N\mu_B$ at 50 kOe, which is close to the saturation value of 2.0 $N\mu_B$ anticipated for a pair of $S = 1/2$ spins with $g = 2$.[12,14] The critical field is ca. 6030 Oe, determined by the peak position of the dM/dH derivative curve at 4 K.

(36) Baker, G. A.; Rushbrooke, G. S.; Gilbert, H. E. *Phys. Rev.* **1964**, *135*, A1272.

The sigmoidal feature of the field-dependent magnetization diminishes when the temperature is at or above 6 K, consistent with the T_N value. No detectable magnetic hysteresis was observed at 2 K as shown in the inset of Figure 11. All of these measurements mentioned above clearly indicate the metamagnetic behavior in **4** with a critical temperature of 6 K and a critical field of ca. 6030 Oe.[12,37]

Conclusions

Four three-dimensional metal−azido coordination polymers were obtained with different amino carboxylic acids as secondary bridging ligands. The results revealed that the addition of different amino carboxylates as coligands leads to a variation of the coordination modes of the azido bridge and different resulting structural topologies of the metal−azido compounds formed. Complex **3** displays an interesting 3,6-connected topological structure that has never been reported previously, and **4** is the first example of coordination polymer with a flexible amino acid as the secondary bridging ligand in metal−azido complexes. Magnetic susceptibility measurements reveal dominant antiferromagnetic couplings for **1** and **3** but a dominant ferromagnetic coupling for **4**, which displays metamagnetic behavior with a magnetic phase transition at a critical temperature of 6 K and transition field of ca. 6030 Oe. The results further confirm the conclusion that the EE azido and syn−anti carboxylato bridges easily induce an antiferomagnetic interaction, and the magnetic interaction through the EO azido bridge has a dependence on the value of the M−N−M bond angle. Moreover, the anti−anti carboxylato bridge in **4** mediates a ferromagnetic interaction.

Acknowledgment. We gratefully thank Prof. Dr. You Song for the discussion of magnetic properties, and we also acknowledge the financial support from the National Natural Science Foundation of China (No. 20461001), Guangxi Natural Science Foundation (No. 0639031), and Ten-hundred-thousand Talents Program in New Century of Guangxi Province, China.

Supporting Information Available: X-ray crystallographic files in CIF format for complexes **1**−**4**, a PDF file containing Figures S1–S8. These materials are available free of charge via the Internet at http://pubs.acs.org.

(37) (a) Monfort, M.; Resino, I.; Ribas, J.; Stoeckli-Evans, H. *Angew. Chem., Int. Ed.* **2000**, *39*, 191–193. (b) Mukherjee, P. S.; Dalai, S.; Chaudhuri, N. R.; Zangrando, E.; Lloret, F. *Chem. Commun.* **2001**, 1444–1445. (c) Gao, E.-Q.; Wang, Z.-M.; Yan, C.-H. *Chem. Commun.* **2003**, 1748–1749. (d) Liu, T.; Zhang, Y.; Wang, Z.; Gao, S. *Inorg. Chem.* **2006**, *45*, 2782–2784. (e) Das, A.; Rosair, G. M.; ElFallah, M. S.; Ribas, J.; Mitra, S. *Inorg. Chem.* **2006**, *45*, 3301–3306.